Three-Dimensional $Bi_2Fe_4O_9$ Nanocubes Loaded on Reduced Graphene Oxide for Enhanced Electromagnetic Absorbing Properties

Min Lu[1], Yuan-Kai Sun[1], Shu-Hao Yang[2], Hui-Ya Wang[2], Xiao-Hui Guan[1]* and Guang-Sheng Wang[2]*

[1] Northeast Electric Power University, Jilin, China, [2] School of Chemistry, Beihang University, Beijing, China

$Bi_2Fe_4O_9$(BFO) nanocubes were prepared in proportion using a simple and easy hydrothermal method, and were then assembled on reduced graphene oxide (rGO) multilayered sheets. The excellent microwave absorption properties of $Bi_2Fe_4O_9$/rGO nanohybrids were achieved by properly adjusting the impedance matching and getting a high attenuation capability contributed from different ratios of the BFO and rGO. A minimum reflection loss value of -61.5 dB at 12.8 GHz was obtained with a $Bi_2Fe_4O_9$/rGO ratio of 2:1, and the broadest bandwidth below -10 dB was up to 5.0 GHz (from 10.8 to 15.8 GHz) with a thickness of 2.4 mm. Additionally, the elementary mechanism of wave absorption performance is also investigated.

Keywords: $Bi_2Fe_4O_9$(BFO) nanocubes, $Bi_2Fe_4O_9$/rGO nanohybrids, wave absorption property, a potential EMW material, hydrothermal method, a rather wide frequency band, synergy effect

INTRODUCTION

Communication equipment, such as mobile phones and fax machines, have brought great convenience to people. At the same time, because of their electromagnetic radiation pollution, they also bring many hidden dangers. In order to address this issue, electromagnetic (EM) wave absorbing materials have attracted an abundance of attention from various fields (Sun et al., 2014; Li et al., 2018a; Liu et al., 2019; Mo et al., 2019). Magnetic materials and their composites are accepted as one of the most significant EM absorbing materials, owing much to their high EM performance, broad frequency range response, low price, easy preparation, and excellent chemical stability (Zhao et al., 2013; Dhawan et al., 2015; Qiu et al., 2017; Tang et al., 2017). However, traditional magnetic metal absorbing materials (Fe, Co, Ni) with a high complex permeability make it difficult to satisfy the impedance match in materials and free space (Xu et al., 2018a). Unlike common magnetic metals, ferrites with a relatively high Snoek's limit, medium-built saturation magnetization, and coercivity have become a popular new EM wave absorbing material (Rusly et al., 2018; Trana et al., 2019; Zhu et al., 2019). For example, Lee et al. Prepared M-type hexaferrites $BaFe_{12-x}Co_xO_{19}$ (x = 0–2), which were synthesized by a co-precipitation technique, in which relatively high reflection loss (RL) values with the frequency range of 0.1–15 GHz was obtained (Trana et al., 2019). Matori et al. used a mechanical activation high energy ball milling (HEBM) method to study the EM properties

of multiferroic $BiFeO_3$ composites under temperatures of 700–800°C (Rusly et al., 2018). Although ferrites have shown immense potential as an EM wave absorbing material, single phase ferrite can still not fully meet the characteristics of being light weight, having a thin thickness, strong absorption, wide absorption bandwidth, and environmental stability. Beyond all doubt, ferrites need to be compounded with other materials to further improve their performance in the field of wave absorption.

To date, there are two main strategies to make ferrite excellent microwave absorbing materials (Liu et al., 2020). Firstly, it is possible to introduce dielectric materials into ferrite becoming an EM compound. Lin et al. fabricated flower-like $MoS_2@Bi_2Fe_4O_9$ MPs with a quite broad bandwidth of 5.0 GHz and a high reflection loss of −52.3 dB (Lin et al., 2018). Yang et al. have successfully prepared a rGO/porous $Bi_2Fe_4O_9$ composite via a dissolution-recrystallization/reduction process, which possesses outstanding EM wave absorption properties and a large absorption bandwidth (Dai et al., 2019). Zhang et al. synthesized a rGO/$BiFeO_3$ composite with the maximum reflection loss value of −46.7 dB (Gao et al., 2019). Secondly, it is also possible to investigate constructional EM materials with special particle structures and microscopic shapes (Feng et al., 2017; Zhang et al., 2018; Huang et al., 2019). For example, Huang et al. prepared $C/CoFe_2O_4$ nanocomposites with a special porous structures root in eggshell membrane, which was shown to have a brilliant EM absorption capability (Huang et al., 2019). Well-bedded $ZnFe_2O_4@SiO_2@rGO$ core-shell microspheres exhibited an outstanding microwave absorption performance (Feng et al., 2017). Such ferrite matrix materials have shown more excellent EM wave absorption properties than single ferrite due to the particular microstructure and the concept of bonding magnetic loss to dielectric loss.

Inspired by of the vast amount of research on two dimensional (2D) materials, rGO represents the unique characteristics needed to acquire unparalleled chemical, physical, and electronic properties because of the electron confinement in dimensions (Zhu et al., 2010; Wang et al., 2011; Guo H. et al., 2013). Furthermore, the fantastically great specific surface area and positive electrical conductivity makes rGO an extremely ideal material to incorporate with magnetic loss materials to acquire effective regulation of EM parameters (Hummers and Offeman, 1958; Guo H. B. L. et al., 2013; Zhang et al., 2013, 2014; Shen et al., 2018; Prasad et al., 2019). Han et al. created a two-step process which involves a hydrothermal reaction and surface modification to obtain the graphene-wrapped ZnO hollow spheres that exhibit an maximum reflection loss of −45.1 dB (Han et al., 2014). One Co_3O_4 nanosheet/rGO composite, which exhibited a reflection loss value of −45.15 dB as well as an effective broad bandwidth of 5.61 GHz, was synthesized (Zhang et al., 2013). Therefore, it can be concluded that the combination of rGO and ferrites with different microstructures is not only able to satisfy the demand of impedance match, which offers an effective way to develop high performance microwave absorbers, but also results in some additional functions which facilitate their practical application in the absorbers.

Separate from the mainstream research on the photocatalysis (Janisse, 2013) and gas sensor properties (Mohapatra et al., 2017) of BFO, this research focuses on the EM wave absorbing ability of BFO. In this work, we prepared an efficient and facile method to synthesize a large amount of three-dimensional BFO nanocubes which easily load on the rGO nanosheets with varying proportions. PVDF was used to function as a disperse matrix due to the synergy effect between dielectric polymer matrixes and parameters that could further improve the EM wave absorption performance of the composites. The exceptional advantages of PVDF, i.e., its flexibility, low weight, and high chemical corrosion resistance, can also benefit the practical applications of the BFO/rGO/PVDF composite absorber (Liu et al., 2015). Moreover, the wave absorption ability of this material has been significantly advanced through the introduction of rGO and the purpose of meeting the optimal impedance match is achieved by changing the ratio of BFO and rGO to adjust the magnetic and dielectric properties of the compound. As expected, an impressive reflection loss of −61.5 dB and a superior frequency band over 5 GHz is achieved by adjusting the proportion of $Bi_2Fe_4O_9$ and rGO to a certain ratio of 2:1 when the thickness of the absorber is just 2.4 mm. Additionally, we have further investigated the mechanism of EMW absorbing properties as well as the influence of dielectric loss, magnetic loss, and impedance match for the materials. To sum up, the method of synthesizing BFO/rGO nanohybrids is simple and efficient and a great EMW absorbing performance can be achieved with a thin thickness which indicates that the BFO/rGO nanohybrids have great potential in practical applications.

EXPERIMENTAL

Fabrication of the Bi2Fe4O9 Nanoparticles and the Bi2Fe4O9/rGO Nanohybrids

Graphene Oxide (GO) was prepared by a modified Hummer's method (Hummers and Offeman, 1958). The synthesis of $Bi_2Fe_4O_9$ nanocubes was conducted via a simple hydrothermal reaction (Han et al., 2006). Briefly, 125 mmol of $Fe(NO_3)_3 \cdot 9H_2O$ and $Bi(NO_3)_3 \cdot 5H_2O$ was added into a 100 mL steel autoclave. Then, a KOH solution of 12 mol/L was slowly poured into the autoclave until 70–80% of its volume stopped. Subsequently, 50 μl of concentrated hydrochloric acid was added into the autoclave. The reaction mixture solution was constantly stirred by the magnetic stirring apparatus for 45 min. After that, the autoclave was placed in the oven at 200°C for 24 h. Finally, the product was washed several times with deionized water and then dried at 60°C in the oven.

The $Bi_2Fe_4O_9$/rGO nanohybrids were synthesized by a non *in situ* composite method. Firstly, the 40 mg of graphene oxide was put in 60 ml of deionized water with ultrasonic treatment for 2 h to obtain a homogeneous dispersion. Then 525 μl of ammonia and 33 μl of hydrazine hydrate were added into the above solution, and then the solution was heated to 90°C while stirring under an oil bath condition. After stirring for 2 h, the solution temperature was reduced to room temperature and then the $Bi_2Fe_4O_9$ nanoparticles were added into the solution, with

constant sonicating for an extra 3 h. Finally, the black mixture was washed several times with the deionized water after collecting by centrifugation and then dried in an oven at 60°C for 12 h to acquire $Bi_2Fe_4O_9$/rGO nanohybrids. The mass ratio between $Bi_2Fe_4O_9$ and rGO were 3:1, 2:1, and 1:1, respectively.

Measurements of Microwave Absorption Properties

The test samples were prepared by mixing the $Bi_2Fe_4O_9$/rGO nanohybrids with the PVDF matrix at a different weight ratio of 10, 20, and 30 wt%. The mixtures were subsequently pressed into concentric annular samples (ϕ_{out} = 7.00 mm and ϕ_{in} = 3.04 mm). To investigate the complex permittivity and permeability values from 2 to 18 GHz, an Agilent N5230C PNA-L Network Analyzer was used with a coaxial wire setup.

Characterization

The morphologies and sizes of the $Bi_2Fe_4O_9$ nanocubes were characterized using a scanning electron microscopy (SEM), a field emission scanning electron microscopy (FE-SEM), and an X-ray diffractometer (XRD) with CuKα radiation. To evaluate Raman spectra, a Laser Raman spectroscopy was adopted. Fourier transform infrared spectra (FT-IR) were obtained by a FT-IR spectrometer (Thermo Scientific) to observe the surface functional groups of GO and rGO. Magnetic properties of $Bi_2Fe_4O_9$ samples were detected under normal conditions by a Vibrating Sample Magnetometer (VSM).

RESULTS AND DISCUSSION

To study the crystalline structure and phase composition of the sample, the XRD pattern of the $Bi_2Fe_4O_9$ sample can be seen in **Figure 1A**. The pure $Bi_2Fe_4O_9$ nanoparticles successfully synthesized by the hydrothermal method are well-crystallized without any impurities and attribute the orthorhombic structure in accordance with the standard data (JSPDS card No.25-0090). From **Figure 1B**, the Raman spectrum shows the typical G band at 1,570 cm^{-1} and D band at 1,340 cm^{-1}. Here, I_D/I_G, which presents the intensity ratio of D band (disordered carbon) to G band (sp^2 carbon), is a common standard for determining the degree of disorder of graphitic layers (Wang et al., 2018; Xu et al., 2018b). According to the Raman spectra in **Figure 1B**, it is not difficult to conclude that the value of I_D/I_G for rGO (1.61) is higher than the value of GO (1.06), reflecting a higher degree of in- plane defect and edge defect in the rGO due to the reduction process. These defects are closely related to the microwave absorption ability of the materials (Wang et al., 2013). The FT-IR spectrum of GO and rGO are given in **Figure 1C** in the range of 500–4,000 cm^{-1}. For pure GO, the broad peak located at about 3,350 cm^{-1} corresponds to O-H stretching vibrations of hydroxyl groups and HOH hydrogen-bonded owing to residual water (Pan et al., 2017; Zhu et al., 2019). The characteristic peak presenting at 1,715 and 1,614 cm^{-1} represent the C = O stretching vibration of carbonyl groups and the C = C skeletal stretching vibration of aromatic carbon. As for the peak at 1,372

FIGURE 1 | (A) XRD image of $Bi_2Fe_4O_9$, **(B)** Raman spectra, **(C)** FTIR spectra of GO and rGO, **(D)** magnetic hysteresis loops of $Bi_2Fe_4O_9$ and all kinds of ratio of BFO: rGO.
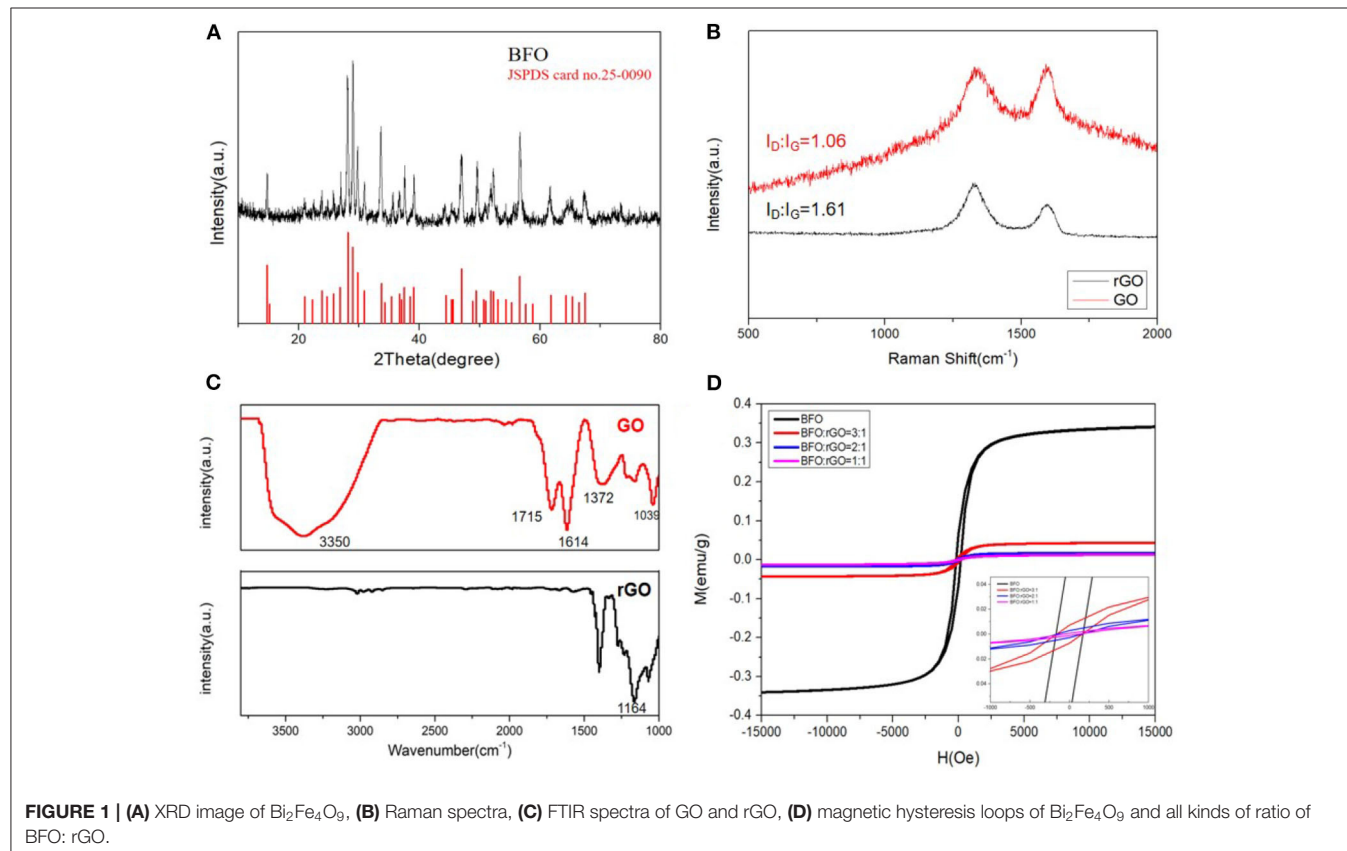
and 1,039 cm^{-1}, this can be considered to be carboxy C-OH stretching vibration and epoxy C-O stretching vibration (Xu et al., 2018b). For rGO, it is obvious that quite a few oxygen-containing functional groups have gone, and the reduction of the hydroxyl peak has exhibited some offset according to the FT-IR spectra, indicating the high reduction of GO. And the new peaks which appeared around 1,164 cm^{-1} are the peak of secondary ammonia produced by hydrazine hydrate in the reduction process. **Figure 1D**, The M-H curves show that the BFO sample is a weakly magnetic substance and with the introduction of rGO, the saturation magnetization decreases further which indicates that dielectric loss plays an important role in Bi$_2$Fe$_4$O$_9$/rGO nanohybrids.

To further observe the microstructure and morphology of Bi$_2$Fe$_4$O$_9$ and Bi$_2$Fe$_4$O$_9$/rGO nanohybrids, the SEM samples were analyzed. **Figures 2a–c** present the SEM image of the BFO sample, which shows the uniform bulk Bi$_2$Fe$_4$O$_9$ cubes with an edge length of 300–800 nm. It is observed that the faces of the Bi$_2$Fe$_4$O$_9$ structures are basically flat, though some of these cubes have a little bit of debris on their surface. Furthermore, cubic structure is the only form, and the particles are more regular and easier to prepare in large quantities. From the FESEM image (**Figure 2d**) for the Bi$_2$Fe$_4$O$_9$/rGO composite, we can easily see that Bi$_2$Fe$_4$O$_9$ cubes with an orderly pore distribution are embedded on the graphene, showing a noticeable 3D bulk-like morphology. To explore the distribution of elements, elemental mappings of Bi$_2$Fe$_4$O$_9$/rGO nanohybrids are displayed in **Figures S1c, S2**. The elemental mapping images indicate that Bi, Fe, O, and C disperse homogeneously in Bi$_2$Fe$_4$O$_9$/rGO nanohybrids. The good dispersion of these nanocubes in rGO may contribute significantly to the EM wave absorption properties.
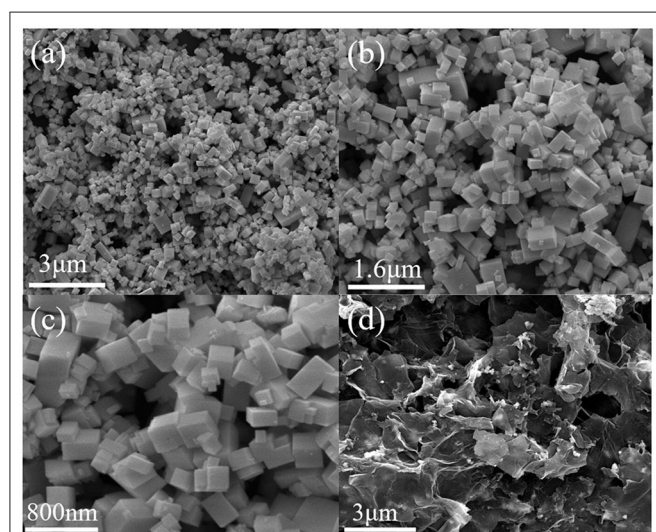
FIGURE 2 | SEM image **(a,b,c)** of Bi$_2$Fe$_4$O$_9$ nanocube, FESEM image **(d)** of Bi$_2$Fe$_4$O$_9$/rGO nanohybrids.

MICROWAVE ABSORPTION PERFORMANCE

To explore the EM wave absorption performance of BFO nanocubes and BFO/rGO nanohybrids, various proportions of the products were mixed with PVDF to form the compounds via a hot-press process (Zhang et al., 2016). The complex permittivity ε_r ($\varepsilon_r = \varepsilon' - j\varepsilon''$) and complex permeability ($\mu_r = \mu' - j\mu''$) for several materials are presented in **Figure 3**. Among them, the complex permittivity real part ε' represents the storage capability of electric energy and the permittivity imaginary part ε'' represents the loss capability of electric energy; complex permeability real part μ' stands for the storage capability of magnetic energy and permeability imaginary part μ'' stands for the dissipation of magnetic energy (Zhou et al., 2017). It can be concluded that the values of ε' and ε'' for all content in the BFO/rGO nanohybrids are much bigger than that of pure phase of BFO in **Figures 3A,B**. As shown in **Figures 3C,D**, the decline of μ' and μ'' for BFO nanoparticles is smooth; at the same time, the decline of μ' and μ'' for all BFO/rGO nanohybrids is also smooth from 6 to 18 GHz, but the value of μ' and μ'' for BFO/rGO nanohybrids shows a sharp decline with increasing frequency from 2 to 6 GHz. The variation curves of the complex permittivity and complex permeability are quite untidy. We suspect this peculiar phenomenon is related to the magnetic loss mechanism.

According to the transmission line theory, the reflection loss (RL) was calculated to study the EM microwave absorption properties, where normalized input characteristic impedance (Z_{in}) is calculated as:(Raghvendra et al., 2018)

$$Zin = \sqrt{\frac{\mu r}{\varepsilon r}} \tanh \left[j \left(2f\pi\, d/c \right) \right] \sqrt{\mu r \varepsilon r} \qquad (1)$$

$$R = 20\log \left| \frac{zin\text{-}1}{zin + 1} \right| \qquad (2)$$

Where c is the velocity of light in free space, d is the thickness of the absorber, and f is the frequency.

From observation, it is clearly shown that the dielectric loss values of all contents of the BFO/rGO nanohybrids are higher than their magnetic loss values in **Figures 4A,B**. Moreover, the dielectric loss values with the filler loading of 20 wt% BFO and 20 wt% BFO/rGO illustrate that the dielectric loss values are enhanced markedly after combining with rGO. There are two dominant common dielectric polarization mechanisms which included space charge polarization and dipolar polarization in the gigahertz frequency range. According to Maxwell-Wagner theory, interfacial polarization, which is also famous as space charge polarization occurs frequently in the composites, were composed of components with various conductivity and permittivity (Zhang et al., 2014). Compared with the weak dielectric loss performance of single BFO, rGO has an excellent dielectric loss due to the dipoles and some residual oxygen functional groups, including epoxy, hydroxyl, and carbonyl groups, which generate more polarization centers and stronger polarization relaxations(Feng et al., 2017). Apparently, BFO/rGO/PVDF composites with two kinds of

FIGURE 3 | Frequency dependence of the **(A)** real part and **(B)** imaginary part of permittivity, **(C)** real part and **(D)** imaginary part of permeability of $Bi_2Fe_4O_9$/rGO nanohybrids with different BFO ratios.

FIGURE 4 | Frequency dependence of dielectric loss **(A)** and magnetic loss **(B)** of samples.
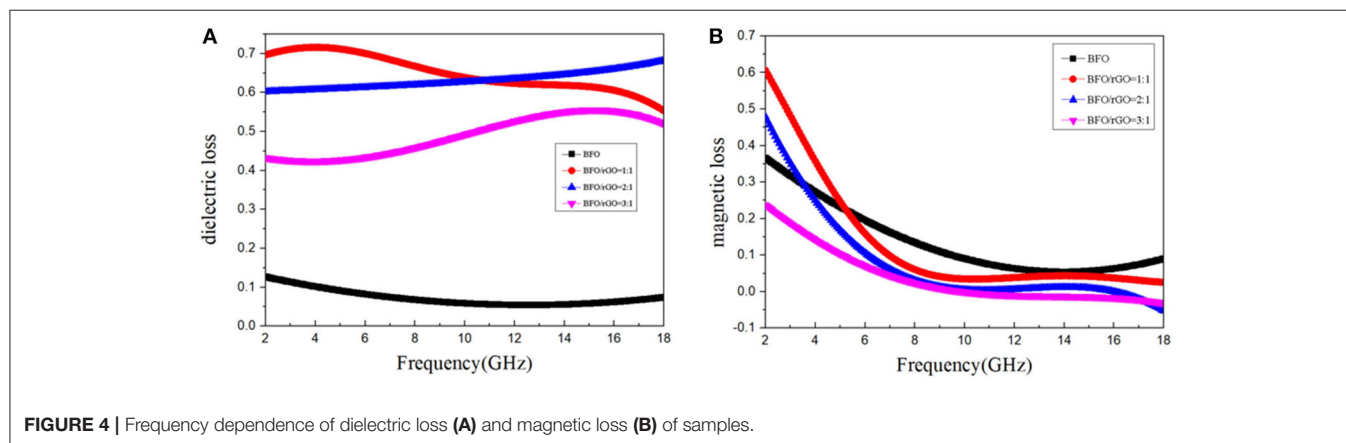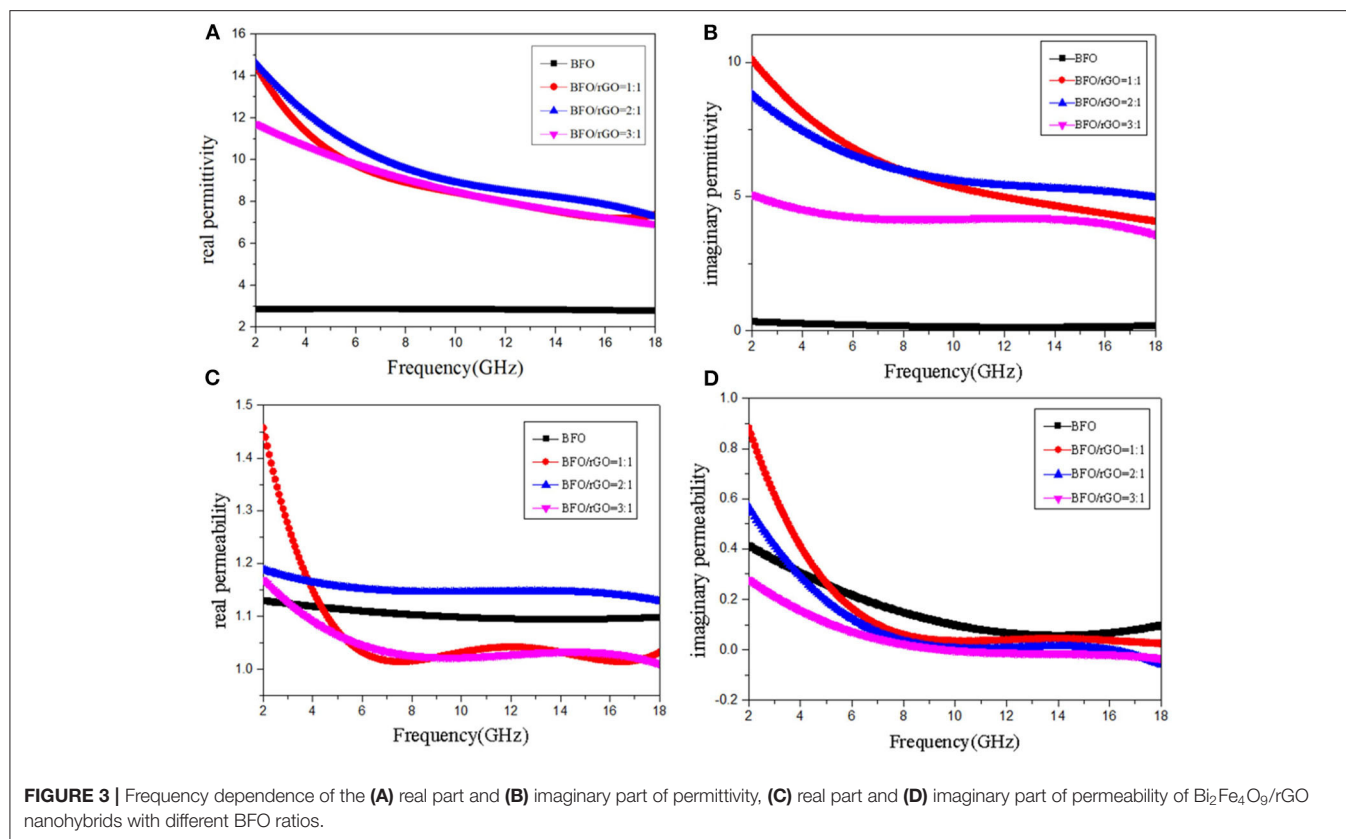
interfaces produced more interfacial polarization than the single interface of the BFO/PVDF composite. Because of the existence of electrophilic fluorine in its molecular structure, PVDF is also a strong dipole material (Prasad et al., 2019). All these conditions mean BFO/rGO have higher dielectric loss values than BFO, which promoted the EM wave absorption. However, the maximum reflection loss peak is not the same frequency as that of the dielectric loss values, which indicates the main dielectric loss mechanism for BFO/rGO nanohybrids includes both dielectric loss and magnetic loss.

For a typical ferrite material, magnetic loss is usually concerned with eddy current effect, natural ferromagnetic

resonance, domain wall resonance, and hysteresis (Li et al., 2018b). Generally, the domain wall resonance only operates at a megahertz frequency range and the hysteresis loss could be negligible in a weak field. Hence, the analysis of magnetic loss for BFO/rGO composites should focus on eddy current effect and natural ferromagnetic resonance. The eddy current loss is calculated by the nether equation:. If the eddy current loss is the reason for the magnetic loss, the C_0 ($C_0 = \mu''(\mu')^{-2} f^{-1}$) would remain constant in the corresponding frequency range (Liu et al., 2019). From the variation tendency of magnetic loss (shown in **Figure 4B**), it can be found that it is same with the decline of μ' and μ''. The decline of magnetic loss for all BFO/rGO

FIGURE 5 | The frequency dependence of **(A)** |Zin/Zo| and **(B)** attenuation coefficient (α) for BFO nanocube and $Bi_2Fe_4O_9$/rGO nanohybrids with a $Bi_2Fe_4O_9$/rGO ratio of 1:1, 2:1, and 3:1.

FIGURE 6 | Illustration of microwave wave absorption mechanisms of the $Bi_2Fe_4O_9$/rGO nanohybrids.
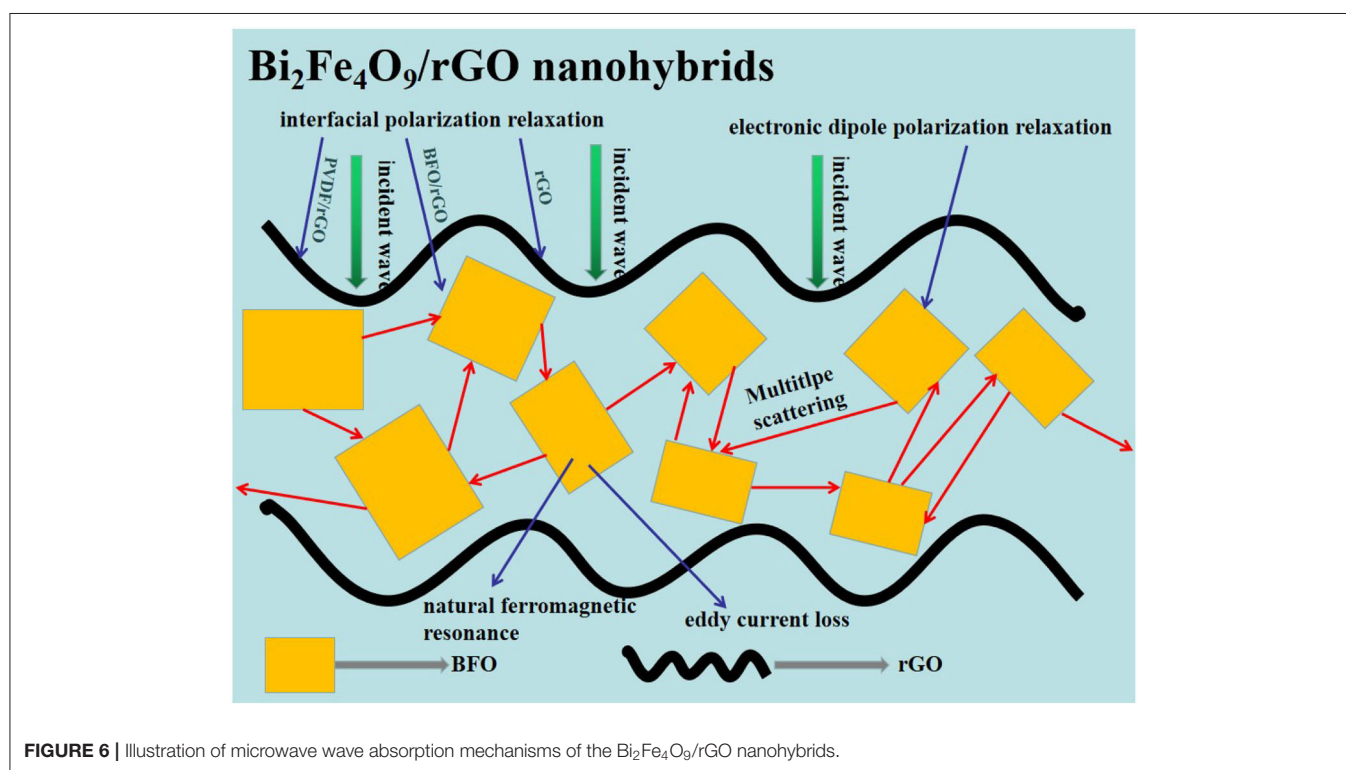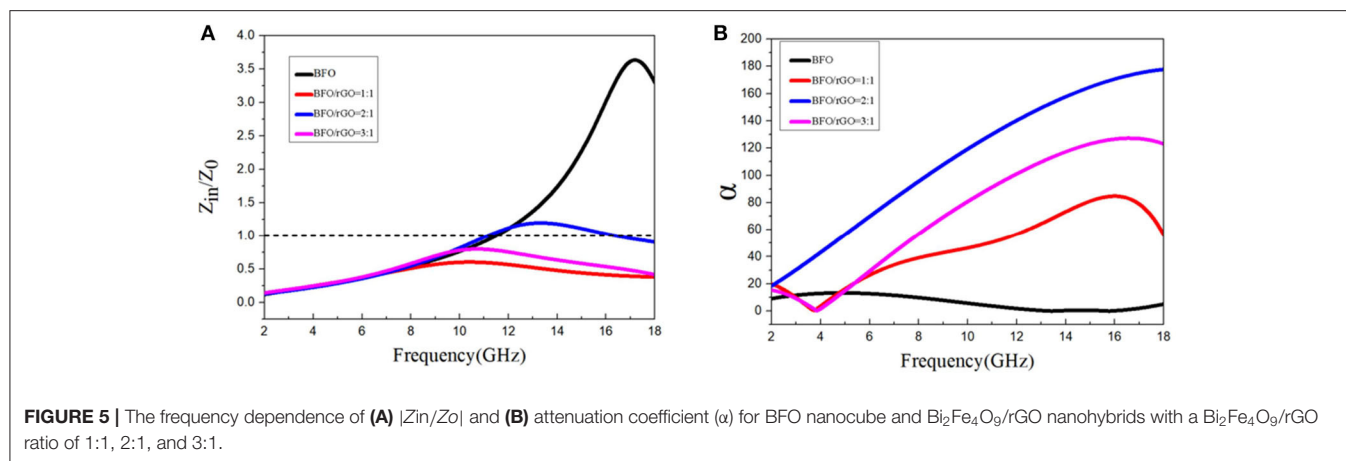
nanohybrids is smooth from 6 to 18 GHz, but the value of magnetic loss shows a sharp decline with increasing frequency from 2 to 6 GHz, which indicates that the main magnetic loss is the eddy current loss. The natural ferromagnetic resonance is related to the enhancement of anisotropic energy (Ha), which can be calculated by the following equation: (Guo et al., 2012)

$$H_a = \frac{4\,|K_1|}{3\mu_0 M_s} \qquad (3)$$

where $|K_1|$ is the anisotropic coefficient and Ms is the saturation magnetization (Zhang et al., 2014). From **Figure 2d**, the Ms value of BFO is higher than that of BFO/rGO, which means

the anisotropic energy of BFO/rGO composites is stronger. The higher anisotropic energy results in the improvement of EM absorption performance, particularly at high frequencies (Zhang et al., 2013, 2014). The results confirmed that eddy current loss and natural ferromagnetic resonance play a common role in regulating the magnetic loss of the BFO/rGO sample.

It is well-known that a good electromagnetic wave absorber must satisfy the two conditions of impedance matching and attenuation characteristic. Impedance matching ratio can be easily understood, as the incident electromagnetic wave can be propagated to the efficient absorber and be converted into heat energy or dissipation through interference, rather than reflecting directly on the surface of absorbers (Chen et al.,

FIGURE 7 | 3D image maps of the reflection loss of all composites (w = 10 wt %). **(A,B,C)** for $Bi_2Fe_4O_9$/rGO nanohybrids with a $Bi_2Fe_4O_9$/rGO ratio of 1:1, 2:1, and 3:1.
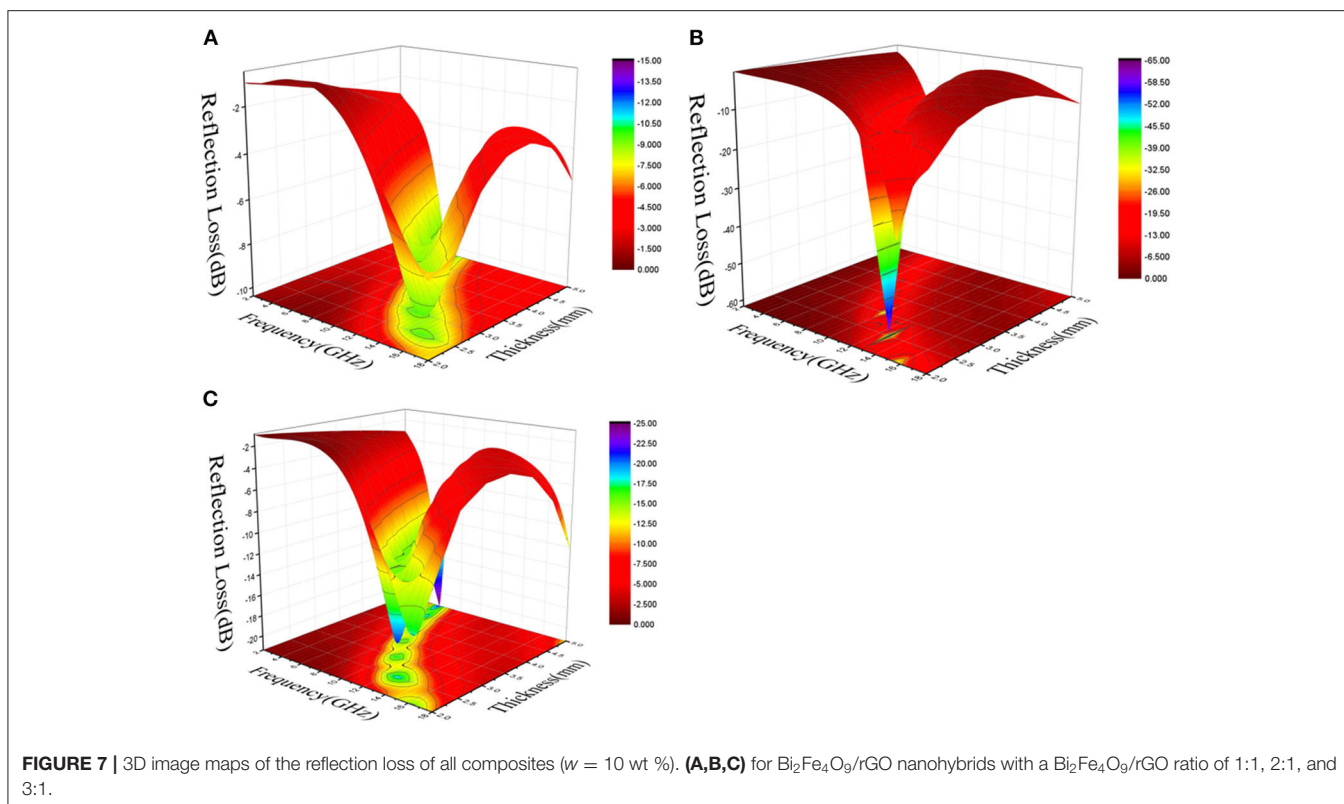
2017; Fang et al., 2017; Li et al., 2018c; Xu et al., 2019). The |Zin/Zo| value, which can be calculated by the above Equation (1), shows impedance matching performance (Chen et al., 2017). The frequency dependence of the |Zin/Zo| value (d = 2.4 mm) of various samples can be observed in **Figure 5A**. Compared with the value of sample BFO, the value of sample BFO/rGO with a ratio of 2:1 is close to 1 in the high frequency region, which means that it has a relatively good impedance matching in the corresponding frequency range. Through **Figure 5A**, it is also proven that it is possible to get a better impedance matching by introducing rGO and changing the ratio of BFO and rGO.

Another factor which is associated with a desirable electromagnetic wave absorption property is electromagnetic attenuation capability, which can be represented by attenuation constant α on the following equation: (Xiang et al., 2014)

$$\alpha = \frac{\sqrt{2}\pi f}{c} \times \sqrt{(\mu''\varepsilon'' - \mu'\varepsilon') + \sqrt{(\mu''\varepsilon'' - \mu'\varepsilon')^2 + (\mu'\varepsilon'' - \mu''\varepsilon')^2}}$$

(4)

Where f is the frequency of the EMW and c is the velocity of light. Hence, excellent microwave absorption performance is related to the combination of impedance matching and high attenuation ability. According to the different ratios of BFO and rGO, adjusting the appropriate basic electromagnetic parameters is conducive to improving the microwave absorption

performance. As shown in **Figure 5B**, because the high dielectric loss and eddy current loss in high frequency, the α value of BFO/rGO samples show an increase trend which BFO samples do not have with increasing frequency. It is also obvious to see the attenuation coefficient value of sample BFO/rGO with a ratio of 1:1 is pretty high; however, it does not have a good microwave absorption performance due to its bad impedance matching. Therefore, the combination of impedance matching and high attenuation ability is an effective way to get an excellent microwave absorption performance as shown in **Figure 6**. The suitable fundamental electromagnetic parameters are adjusted by changing the contents of the BFO and rGO, which are beneficial to enhancing microwave absorption performance.

Figures 7A–C show the three-dimensional images of calculated theoretical RLs of the BFO/rGO nanohybrids at different thicknesses (1–5 mm) in the frequency range of 2–18 GHz with the filler loading of 10 wt% with the ratio of BFO/rGO, 1:1, 2:1; and 3:1, respectively. Meanwhile, it is not hard to see that we can regulate the ability of BFO/rGO composites to absorb electromagnetic waves by adjusting the ratio of the BFO and rGO. Since the reflection loss properties are very sensitive to the content of rGO in BFO/rGO nanohybrids, **Figure 8** shows the calculated RLs for the BFO/rGO absorber with thicknesses varying from 1 to 5 mm in the frequency range of 2–18 GHz with the filler loading of 5, 10, 15, and 20 wt% with a BFO/rGO ratio of 2:1. Compared with **Figure 8** and **Figure S3**, with the introduction of rGO, the microwave absorption performances

FIGURE 8 | RL curves of the composites with the thickness of 1–5 mm in the frequency range of 2–18 GHz for $Bi_2Fe_4O_9$/rGO nanohybrids with $Bi_2Fe_4O_9$/rGO ratio of 2:1 under different filler loading. **(A)**: 5% wt, **(B)**: 10% wt, **(C)**: 15% wt, **(D)**: 20% wt.
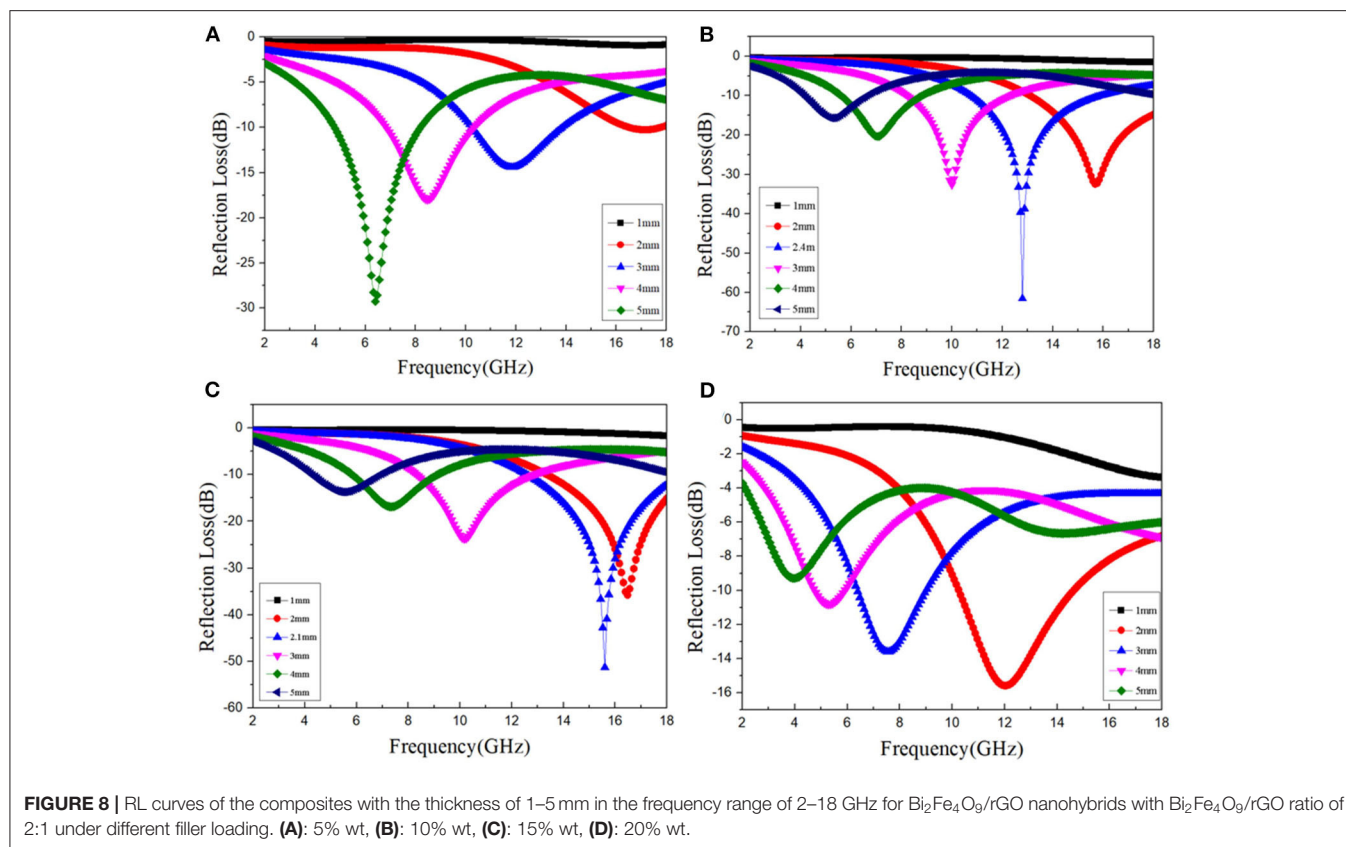
of composites are largely enhanced. Meanwhile, all the minimal RL values are <-10 dB in **Figures 8A–C** with thicknesses of 2–5 mm. When the ratio of BFO/rGO is 1:1, optimal RL value reaches −40 dB at a pretty high frequency with a relatively small bandwidth in **Figure S4c**, but the minimum RLs gradually turn to a low frequency range with the increasing thickness. The effective absorption bandwidth below −10 dB for the three absorbers can cover 4.0–18.0 GHz in **Figure 8C** and **Figures S4c**, **S5c**, respectively. From **Figure 8B**, one outstanding microwave absorption property with an optimal RL value of −61.5 dB and a broad effective bandwidth of 5 GHz (10.8–15.8 GHz), and a thin matched thickness of 2.4 mm, is achieved with the ratio BFO/rGO of 2:1. It is not difficult to see that the microwave absorbing ability of the BFO/rGO nanohybrids at various frequencies can be regulated by changing the ratio of the rGO and BFO through **Figure 8** and **Figures S4**, **S5**. Furthermore, we can conclude that, with the increase of thicknesses of 2–5 mm in **Figure 8** and **Figures S4**, **S5**, the maximum peak value develops to a low frequency when increasing the thickness, which indicates BFO/rGO/PVDF composites will become a potential excellent microwave absorption material.

CONCLUSION

We have synthesized three-dimensional bulk $Bi_2Fe_4O_9$ nanocubes using a simple hydrothermal method, and the

$Bi_2Fe_4O_9$ nanoparticles successfully loaded on graphene forming a BFO/rGO/PVDF composite absorber. It is proven that it is a positive way to obtain a potential EMW material by combining BFO, rGO, and PVDF. Specifically, the introduction of rGO sheets and PVDF dramatically ameliorated the impedance matching of BFO because of the synergy effect between multiple components. When the ratio of $Bi_2Fe_4O_9$ to rGO reaches 2:1 with an absorber thickness of 2.4 mm, the composite reaches −61.5 dB at 12.8 GHz, possessing a rather wide frequency band of 10.8–15.8 GHz (RL <-10 dB). Moreover, the thickness of the absorber is a pivotal factor in practical applications, meaning that $Bi_2Fe_4O_9$/rGO nanohybrids are very significant for developing thin EM wave absorbing materials. Therefore, the composite has a broad application prospect in the field of microwave absorption.

DATA AVAILABILITY STATEMENT

The raw data supporting the conclusions of this article will be made available by the authors, without undue reservation.

AUTHOR CONTRIBUTIONS

ML and Y-KS: data curation and writing- original draft preparation. S-HY and H-YW: conceptualization, methodology,

visualization, and investigation. X-HG and G-SW: supervision. All authors contributed to the article and approved the submitted version.

FUNDING

SUPPLEMENTARY MATERIAL

The Supplementary Material for this article can be found online at: https://www.frontiersin.org/articles/10.3389/fchem. 2020.00608/full#supplementary-material

REFERENCES

Chen, H., Huang, Z., Huang, Y., Zhang, Y., Ge, Z., and Qin, B. (2017). Synergistically assembled MWCNT/graphene foam with highly efficient microwave absorption in both C and X bands. *Carbon* 124, 506–514. doi: 10.1016/j.carbon.2017.09.007

Dai, J. J., Yang, H. B., Wen, B., Zhou, H. W., Wang, L., and Lin, Y. (2019). Flower-like $MoS_2@Bi_2Fe_4O_9$ microspheres with hierarchical structure as electromagnetic wave absorber. *Appl. Surf. Sci.* 479, 1226–1235. doi: 10.1016/j.apsusc.2019.02.049

Dhawan, R., Saroj, K.umari, Kumar, R., Dhawanb, S. K., and Dhakate, S. R. (2015). Mesocarbon microsphere composites with Fe_3O_4 nanoparticles for outstanding electromagnetic interference shielding effectiveness. *RSC Adv.* 54, 43279–43289. doi: 10.1039/C5RA03332B

Fang, J. S., Huang, D., Lv, R., Bai, Y., Huang, Z. H., and Gu, J. (2017). Three-dimensional reduced graphene oxide powder for efficient microwave absorption in the S band (2-4 GHz). *RSC Adv.* 7, 25773–25779. doi: 10.1039/C7RA03215C

Feng, J., Hou, Y., Wang, Y., and Li, L. (2017). Synthesis of hierarchical $ZnFe_2O_4@SiO_2@RGO$ core-shell microspheres for enhanced electromagnetic wave absorption. *ACS Appl. Mater. Interfaces* 9, 14103–14111. doi: 10.1021/acsami.7b03330

Gao, X., Wang, Y., Wang, Q. G., Wu, X. M., Zhang, W. Z., Zong, M., et al. (2019). Facile synthesis of a novel flower-like $BiFeO_3$ microspheres/graphene with superior electromagnetic wave absorption performances. *Ceram Int.* 45, 3325–3332. doi: 10.1016/j.ceramint.2018.10.243

Guo, H., Zhan, Y. Q., Chen, Z. R., and Meng, F. B. (2013). Decoration of basalt fibers with hybrid Fe_3O_4 microspheres and their microwave absorption application in bisphthalonitrile composites. *J. Mater. Chem. A* 1, 2286–2296. doi: 10.1039/C2TA00562J

Guo, H. B. L., Su, P., Kang, X., and Ning, S. K. (2013). Synthesis and characterization of nitrogen-doped graphene hydrogels by hydrothermal route with urea as reducing-doping agents. *J. Mater. Chem. A* 6, 2248–2255. doi: 10.1039/C2TA00887D

Guo, J., Wang, X., Miao, P., Liao, X., Zhang, W., and Shi, B. (2012). Onestep seeding growth of controllable Ag@Ni core–shell nanoparticles on skin collagen fiber with introduction of plant tannin and their application in high-performance microwave absorption. *J. Mater. Chem.* 22, 11933–11942. doi: 10.1039/c2jm30370a

Han, J. T., Huang, Y. H., and Huang, W. (2006). Tunable synthesis of bismuth ferrites with various morphologies. *Adv. Mater.* 18, 2145–2148. doi: 10.1002/adma.200600072

Han, M., Yin, X. W., Kong, L., and Li, M. (2014). Graphene-wrapped ZnO hollow spheres with enhanced electromagnetic wave absorption properties. *J. Mater. Chem. A.* 2, 16403–16409. doi: 10.1039/C4TA03033H

Huang, L., Li, J. J., Wang, Z. J., Li, Y. B., He, X. D., and Yuan, Y. (2019). Microwave absorption enhancement of porous $C@CoFe_2O_4$ nanocomposites derived from eggshell membrane. *Carbon* 143, 507–516. doi: 10.1016/j.carbon.2018.11.042

Hummers, W. S., Jr., and Offeman, R. E. (1958). Preparation of graphitic oxide. *J. Am. Chem. Soc.* 80, 1339–1939. doi: 10.1021/ja01539a017

Janisse, P. (2013). Preparation of $Bi_2Fe_4O_9$ particles by hydrothermal synthesis and functional properties. *Phase Transit* 86, 726–736. doi: 10.1080/01411594.2012.741238

Li, H., Bao, S., Li, Y., Huang, Y., Chen, J., Zhao, H., et al. (2018a). Optimizing the electromagnetic wave absorption performances of designed $Co_3Fe_7@C$ yolk-shell structures. *ACS Appl. Mater. Interfaces* 34, 28839–28849. doi: 10.1021/acsami.8b08040

Li, H., Cao, Z., Lin, J., Zhao, H., Jiang, Q., Jiang, Z., et al. (2018b). Synthesis of u-channelled spherical $Fe_x(Co_yNi_{1−y})_{100−x}$ Janus colloidal particles with excellent electromagnetic wave absorption performance. *Nanoscale* 10, 1930–1938. doi: 10.1039/C7NR06956A

Li, X., Yin, X., Song, C., Han, M., Xu, H., Duan, W., et al. (2018c). Self-assembly core-shell graphene-bridged hollow MXenes spheres 3D foam with ultrahigh specific EM absorption performance. *Adv. Funct. Mater.* 28:1803938. doi: 10.1002/adfm.201803938

Lin, Y., Dai, J. J., Yang, H. B., Wang, L., and Wang, F. (2018). Graphene multilayered sheets assembled by porous $Bi_2Fe_4O_9$ microspheres and the excellent electromagnetic wave absorption properties. *Chem. Eng. J.* 334, 1740–1748. doi: 10.1016/j.cej.2017.11.150

Liu, P. B., Zhang, Y. Q., Yan, J., Huang, Y., Xia, L., and Guang, Z. X. (2019). Synthesis of lightweight N-doped graphene foams with open reticular structure for high-efficiency electromagnetic wave absorption. *Chem. Eng. J.* 368, 285–298. doi: 10.1016/j.cej.2019.02.193

Liu, X. F., Cui, X. R., Chen, Y. X., Zhang, X. J., Yu, R. H., Wang, G. S., et al. (2015). Modulation of electromagnetic wave absorption by carbon shell thickness in carbon encapsulated magnetite nanospindles–poly(vinylidene fluoride) composites. *Carbon* 95, 870–878. doi: 10.1016/j.carbon.2015.09.036

Liu, Y., Shu, R. W., Kong, L. B., Zhou, J., Shu, X., Wang, J., et al. (2020). Enhanced microwave absorption properties of $(1–x)CoFe_2O_4/xCoFe$ composites at multiple frequency bands. *J. Magn. Magn. Mater.* 493:165699. doi: 10.1016/j.jmmm.2019.165699

Mo, Z. C., Yang, R. L., Lu, D. W., and Yang, L. L. (2019). Lightweight, three-dimensional carbon Nanotube@TiO_2 sponge with enhanced microwave absorption performance. *Carbon* 144, 433–439. doi: 10.1016/j.carbon.2018.12.064

Mohapatra, S. R., Vishwakarma, P. N., Kaushik, S. D., Choudhary, R. J., Mohapatra, N., and Singh, A. K. (2017). Cobalt substitution induced magnetodielectric enhancement in multiferroic Bi2Fe4O9. *J. Appl. Phys.* 121:124101. doi: 10.1063/1.4979094

Pan, H., Xu, M., Qi, Q., and Liu, X. (2017). Facile preparation and excellent microwave absorption properties of an RGO@$Co_{0.33}Ni_{0.67}$ lightweight absorber. *RSC Adv.* 7, 43831–43838. doi: 10.1039/C7RA06849B

Prasad, J., Singh, A. K., Tomar, M., Gupta, V., and Singh, K. (2019). Strong electromagnetic wave absorption and microwave shielding in the Ni–Cu@MoS_2/rGO composite. *J. Mater. Sci.* 30, 18666–18677. doi: 10.1007/s10854-019-02219-7

Qiu, X., Wang, L., Zhu, H., Guan, Y., and Zhang, Q. (2017). Lightweight and efficient microwave absorbing materials based on walnut shell-derived nano-porous carbon. *Nanoscale* 9, 7408–7418. doi: 10.1039/C7NR02628E

Raghvendra, K. M., Aastha, D., Priyanka, M., and Sabu, T. (2018). "Electromagnetic interference shielding materials for aerospace application: a state of the art," in *Advanced Materials for Electromagnetic Shielding: Fundamentals, Properties, and Applications (John Wiley & Sons)*, 327–365. doi: 10.1002/9781119128625.ch15

Rusly, S. N. A., Matori, K. A., Ismail, I., Abbas, Z., Awang, Z., Idris, F. M., et al. (2018). Effects of crystalline phase formation of multiferroic $BiFeO_3$ on microwave absorption characteristics. *J. Mater. Sci.* 15, 13229–13240. doi: 10.1007/s10854-018-9447-8

Shen, W., Ren, B., Wu, S., Wang, X., and Zhou, X. (2018). Facile synthesis of rGO/$SmFe_5O_{12}$/$CoFe_2O_4$ ternary nanocomposites: composition control for

superior broadband microwave absorption performance. *Appl. Surf. Sci.* 453, 464–476. doi: 10.1016/j.apsusc.2018.05.150

Sun, D., Zou, Q., Wang, Y., Jiang, W., and Li, F. (2014). Controllable synthesis of porous Fe_3O_4@ZnO sphere decorated graphene for extraordinary electromagnetic wave absorption. *Nanoscale* 12, 6557–6562. doi: 10.1039/C3NR06797A

Tang, J. M., Liang, N., Wang, L., Li, J., Tian, G., Zhang, D., et al. (2017). Three-dimensional nitrogen-doped reduced graphene oxide aerogel decorated with Ni nanoparticles with tunable and unique microwave absorption. *Carrbon* 152, 575–586. doi;10.1016/j.carbon.2019.06.049

Trana, N., Choia, Y. J., Phana, T. L., Yangb, D. S., and Lee, B. W. (2019). Electronic structure and magnetic and electromagnetic wave absorption properties of $BaFe_{12-x}Co_xO_{19}$ M-type hexaferrites. *Curr. Appl. Phys.* 12, 1343–1348. doi: 10.1016/j.cap.2019.08.023

Wang, C., Han, X., Xu, P., Zhang, X., Du, Y., Hu, S., et al. (2011). The electromagnetic property of chemically reduced graphene oxide and its application as microwave absorbing material. *Appl. Phys. Lett.* 4:046101. doi: 10.1063/1.3555436

Wang, C., Murugadoss, V., Kong, J., He, Z. F., Ma, X. M., and Guo, L. (2018). Overview of carbon nanostructures and nanocomposites for electromagnetic wave shielding. *Carbon* 140, 696–733. doi: 10.1016/j.carbon.2018.09.006

Wang, D., Zhang, X., Zha, J. W., Zhao, J., Dang, Z. M., and Hu, G. H. (2013). Dielectric properties of reduced graphene oxide/polypropylene composites with ultralow percolation threshold. *Polymer* 54, 1916–1922. doi: 10.1016/j.polymer.2013.02.012

Xiang, J., Li, J., Zhang, X., Ye, Q., Xu, J., and Shen, X. (2014). Magnetic carbon nanofibers containing uniformly dispersed Fe/Co/Ni nanoparticles as stable and highperformance electromagnetic wave absorbers. *J. Mater. Chem. A* 2, 16905–16914. doi: 10.1039/C4TA03732D

Xu, H., Yin, X., Li, X., Li, M., Liang, S., Zhang, L., et al. (2019). Lightweight Ti_2CTX MXene/poly(vinyl alcohol) composite foams for electromagnetic wave shielding with absorption-dominated feature. *ACS Appl. Mater. Interfaces* 11, 10198–10207. doi: 10.1021/acsami.8b21671

Xu, W., Pan, Y. F., Wei, W., Wang, G. S., and Qu, P. (2018a). Microwave absorption enhancementand dual-nonlinear magnetic resonanceof ultrasmallnickel with Quasi-one-dimensional nanostructure. *Appl. Surf. Sci.* 428, 54–60. doi: 10.1016/j.apsusc.2017.09.052

Xu, W., Wang, G. S., and Yin, P. G. (2018b). Designed fabrication of reduced graphene oxides/Ni hybrids for effective electromagnetic absorption and shielding. *Carbon* 139, 759–767. doi: 10.1016/j.carbon.2018.07.044

Zhang, G., Shu, R., Xie, Y., Xia, H., Gan, Y., Shi, J., et al. (2018). Cubic $MnFe_2O_4$ particles decorated reduced graphene oxide with excellent microwave absorption properties. *Mater. Lett.* 231, 209–212. doi: 10.1016/j.matlet.2018.08.055

Zhang, X. J., Wang, G. S., Cao, W. Q., Wei, Y. Z., Liang, J. F., Guo, L., et al. (2014). Enhanced microwave absorption property of reduced graphene oxide (RGO)-$MnFe_2O_4$ nanocomposites and polyvinylidene fluoride. *ACS Appl. Mater. Interfaces* 6, 7471–7478. doi: 10.1021/am500862g

Zhang, X. J., Wang, G. S., Wei, Y. Z., Guo, L., and Cao, M. S. (2013). Polymer-composite with high dielectric constant and enhanced absorption properties based on graphene–CuS nanocomposites and polyvinylidene fluoride. *J. Mater. Chem. A* 39, 12115–12122. doi: 10.1039/c3ta12451g

Zhang, X. J., Wang, G. S., and Zhu, J. L. (2016). Enhanced microwave absorption material of ternary nanocomposites based on $MnFe_2O_4$@SiO_2, polyaniline and polyvinylidene fluoride. *RSC Adv.* 6, 88104–88109. doi: 10.1039/c6ra17076e

Zhao, X., Zhang, Z., Wang, L., Xi, K., Cao, Q., Wang, D., et al. (2013). Excellent microwave absorption property of Graphene-coated Fe nanocomposites. *Sci. Rep.* 3:3421. doi: 10.1038/srep03421

Zhou, N., An, Q., Xiao, Z., Zhai, S., and Shi, Z. (2017). Solvothermal synthesis of three-dimensional, Fe_2O_3 NPs-embedded CNT/N-doped graphene composites with excellent microwave absorption performance. *RSC Adv.* 71, 45156–45169. doi: 10.1039/C7RA06751H

Zhu, T., Chang, S., Song, Y. F., Lahoubi, M., and Wang, W. (2019). PVP-encapsulated $CoFe_2O_4$/rGO composites with controllable electromagnetic wave absorption performance. *Chem. Eng. J.* 373, 755–766. doi: 10.1016/j.cej.2019.05.079

Zhu, Y., Murali, S., Cai, W., Li, X., Suk, J. W., Potts, J. R., et al. (2010). Graphene and graphene oxide: synthesis, properties, and applications. *Adv. Mater.* 35, 3906–3924. doi: 10.1002/adma.201001068